Japanese Journal of Applied Physics 51 (2012) 06FC05 **REGULAR PAPER**
DOI: 10.1143/JJAP.51.06FC05

Study of Development Processes for ZEP-520 as a High-Resolution Positive and Negative Tone Electron Beam Lithography Resist

Mohammad Ali Mohammad[1]*, Kirill Koshelev[1,2], Taras Fito[1,2], David Ai Zhi Zheng[1], Maria Stepanova[1,2], and Steven Dew[1]

[1] *Department of Electrical and Computer Engineering, University of Alberta, Edmonton, AB T6G 2V4, Canada*
[2] *National Institute for Nanotechnology NRC, 11421 Saskatchewan Drive, Edmonton, AB T6G 2M9, Canada*

Received November 30, 2011; revised January 24, 2012; accepted February 8, 2012; published online June 20, 2012

ZEP brand electron beam resists are well-known for their high sensitivity and etch durability. The various performance metrics such as sensitivity, contrast, and resolution of ZEP resist depend strongly on the development process. In this work, we investigate the development of ZEP-520 resist through contrast curves, dense gratings, and surface roughness measurements using three different classes of developer systems of varying solvation strength, ZED-N50, methyl isobutyl ketone (MIBK) : isopropyl alcohol (IPA) 1 : 3, and IPA : H_2O 7 : 3, at the ambient temperature (22 °C) and cold (−15 °C) development conditions. In order to provide a deeper insight into the ZEP development process, we propose a novel kinetic model of dissolution for ZEP, and develop an efficient analytical method that allows determining the microscopic parameters of ZEP dissolution based on experimental contrast curves. We also observe experimentally and characterize the negative tone behavior of ZEP for dense grating patterning and compare its performance with positive tone behavior.
© 2012 The Japan Society of Applied Physics

1. Introduction

Electron beam lithography (EBL) is the technology of choice for serial prototyping and fabrication of nanoscale features and devices. In EBL, a focused beam of electrons induces a chemical change in a radiation sensitive material (resist) such as chain-scissioning,[1–3] cross-linking,[4–6] or both[7–11] depending on various process variables used. These process variables include exposure and development stage conditions such as the exposure voltage and dose, developer selection, development time and temperature, etc. The tuning of these variables yields a variety of useful fabrication processes as well as allows investigation of the underlying physico-chemical mechanisms. A range of metrics exist for evaluating a particular process such as the sensitivity, resolution, surface roughness, line edge roughness, etc.

ZEP brand co-polymer (1 : 1 α-chloromethacrylate and α-methylstyrene) positive-tone electron beam resists (Nippon Zeon) have been known for their higher sensitivity and etch durability compared to the conventional poly-(methyl methacrylate) (PMMA) resist for nearly two decades.[12] The higher sensitivity and etch durability of ZEP are attributed to the presence of the chlorine and phenyl groups, respectively.[13] The two commonly available formulations for ZEP brand resist are ZEP-520 and ZEP-7000; the main difference being the molecular weights of 67 and 476 kg/mol, respectively.[14] The higher molecular weight formulation is understood to yield a higher contrast at the cost of resist swelling; however, these differences are strongly dependent on the processing conditions employed. In this study, the examined formulation is ZEP-520, in continuation with our previous study.[15] The manufacturer recommended developer for ZEP-520 is composed of a single-solvent compound n-amyl acetate, marketed as ZED-N50.[16]

In our present study, we investigate the development stage variables — the selection of the developer, development time, and temperature. A survey of literature indicates that a large number of single-solvent and binary-solvent developers have been used for ZEP. Single-solvent developers include compounds such as xylenes[17] and alkyl-acetates (methyl, ethyl, ..., octyl).[14,17,18] Binary-solvent developers include mixtures of xylenes and dioxane,[12] hexane and acetates, butanone, and dichlorobenzene in various ratios.[14,18] Furthermore, some of the above developers (primarily acetate based formulations) have also been chilled prior to the development step down to 3,[19] −10,[20] −17,[21] −20,[22] −40,[22] and −50 °C[23,24] in various studies. The dose-to-clear for ZEP has been shown to saturate at a development temperature of −20 °C, which is very close to the result of −15 °C obtained for PMMA.[25,26]

Previously,[15] we began exploring the room temperature behavior of other classes of binary-developers methyl isobutyl ketone (MIBK) : isopropyl alcohol (IPA) 1 : 3 and IPA : H_2O 7 : 3, in addition to the standard ZED-N50 for fabricating dense grating patterns in ZEP and PMMA and proposed various modeling schemes to describe exposure and development of ZEP. In this work on ZEP resist, we extend our study to cold development −15 °C conditions, obtain contrast curves for various developer and development conditions, and study both the positive and negative tone behavior of ZEP through contrast curves, dense grating fabrication, and atomic force microscopy (AFM) studies. A distinguishing aspect of this work is the presentation of a novel kinetic model of ZEP resist development and parameterization method using the experimental contrast curves that can be extended to numerous resist-developer systems. For the negative tone behavior of ZEP, we provide a detailed dense grating fabrication study, not available in literature previously.

2. Experiment

In order to evaluate alternative developers for positive and negative tone ZEP behavior, we conducted two different sets of experiments. One set of experiments was designed for obtaining contrast curves and the other for obtaining dense grating patterns of a moderate aspect ratio. Except for resist thickness and exposure pattern design, all the experimental conditions were kept uniform in both sets of experiments.

To obtain contrast curves, an array of 1 μm squares with a gradually increasing dose were exposed by 10 keV electrons (Raith 150/150[TWO]) on a 145–160 nm thick ZEP-520 resist

*E-mail address: M.A.Mohammad@ualberta.net

 © 2012 The Japan Society of Applied Physics

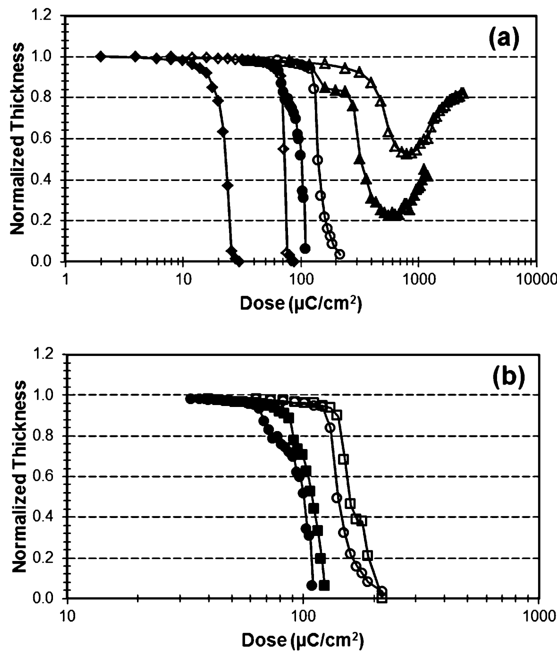

Fig. 1. Normalized contrast curves for 160 nm thick ZEP-520, exposed at 10 keV, and developed at 22 °C (filled symbols) and −15 °C (open symbols). (a) Comparison of ZED-N50 (diamonds), MIBK : IPA 1 : 3 (circles), and IPA : H_2O 7 : 3 (triangles) developers for 20 s development. (b) Comparison of 5 s (square) and 20 s (circles) development using MIBK : IPA 1 : 3 developer.

layer. Each adjacent square was given a minimum spacing of 2 μm to reduce the proximity effect. The exposed resist was developed for 5 and 20 s at 22 °C (room temperature: RT) and at −15 °C in three developer/rinse combinations: (a) ZED-N50 + 20 s IPA, (b) MIBK : IPA 1 : 3 + 20 s IPA, (c) IPA : H_2O 7 : 3 + no rinse. The rinse was kept at the same temperature as the developer. The resulting resist surface was scanned by an AFM (Veeco Dimension 3100). The AFM surface scans are used to accurately assess depth variation with increasing dose. Examples of the resulting contrast curves are shown in Figs. 1(a) and 1(b). In addition, high resolution AFM scans of the exposed area are used to assess surface roughness and image fine details of the partially exposed resist to learn more about the dissolution stage.

In order to assess the viability of the aforementioned developers for obtaining dense gratings, arrays of 40, 50, 60, and 70 nm pitch gratings were exposed by 10 keV electrons (Raith 150/150$^{\text{TWO}}$) on a 60–64 nm thick ZEP-520 resist layer. Each grating array includes a minimum of 2000 adjacent single pixel lines with a progressively increasing dose covering a $10 \times 50\,\mu\text{m}^2$ field to capture the complete contribution of any proximity effects. Numerous grating arrays were exposed with increasing dose factors in order to expose the resist from <100 pC/cm to >17,000 pC/cm dose. This wide range of exposure doses allows us to study, in detail, the behavior of ZEP resist with increasing dose. We are able to witness the various grating morphologies and obtain the positive and negative tone dose windows. The development conditions were identical to those described in the contrast curve study above. The patterned resist was imaged by an SEM (Hitachi S-4800), and the critical dimension measurements were conducted using ImageJ[27] and a locally written script.

3. Theory

To efficiently co-optimize the multitude of various factors on which the EBL process depends, it is highly desirable to have a theoretical tool to predict the performance of resist and developer under particular conditions. Earlier[15,28,29] we introduced a model which represents dissolution of a positive-tone resist by a kinetic diffusion-driven process. Based on this model,[15] dissolution of a uniformly exposed resist can be described by

$$\frac{dz}{dt} = \frac{D(z)}{z}, \tag{1}$$

where t is time of dissolution, z is depth reached at time t, and the effective diffusivity $D(z)$ is given by[28]

$$D(z) = \langle n \rangle^{-\alpha} \beta_0 \exp\left(-\frac{\Delta U}{kT}\right). \tag{2}$$

In eq. (2), ΔU is activation energy, n is the number of monomers in resist fragments, and the averaging is performed over the fragment size distribution in exposed resist at depth z. One can demonstrate that for moderate applied doses, when $\langle n \rangle \propto 1/d$, the expression for diffusivity becomes

$$D(z) = cp^{\alpha}(z) d^{\alpha} \exp\left(-\frac{\Delta U}{kT}\right), \tag{3}$$

see for example ref. 28. In eq. (3) d is dose, $p(z)$ is the yield of the main-chain scissions per electron at depth z, and c is a proportionality coefficient. The parameter α in eq. (3) determines the dependence of the diffusivity on the exposure, and can be considered as a characteristic of the resist's contrast.

Here we propose a new methodology to parameterize the model [eqs. (1)–(3)] so that it reproduces the experimental data for ZEP. In our approach, we derive simple equations that allow the determination of some of the parameters in eq. (3) employing the experimental contrast curves collected for different temperatures and times of development. In the model, we consider a uniform exposure of the resist, and assume that dissolution can be described by a gradual increase of depth z. Initially $z = 0$, whereas complete resist clearance corresponds to $z = z_{\max}$. Equation (1), which describes such a process, can be easily integrated. For example,

$$\int_0^{z_{\max}} \frac{z\,dz}{p^{\alpha}(z)} = c \exp\left(-\frac{\Delta U}{kT}\right) d^{\alpha} t_{\max}, \tag{4}$$

where $t_{\max}$ is time required to clear the resist. Equation (4) can be generalized to the case of arbitrary initial and final dissolution depths z_1 and z_2 such that $0 \le z_1 < z_2 \le z_{\max}$:

$$\int_{z_1}^{z_2} f(z)\,dz = c \exp\left(-\frac{\Delta U}{kT}\right) d^{\alpha} \Delta t, \tag{5}$$

where $f(z) = z/p^{\alpha}(z)$ and Δt is time required for dissolution from depth z_1 to z_2. For two samples exposed at the same voltage with different doses, and developed up to the same depths with the same developer, but with different development temperatures, one can write,

 © 2012 The Japan Society of Applied Physics

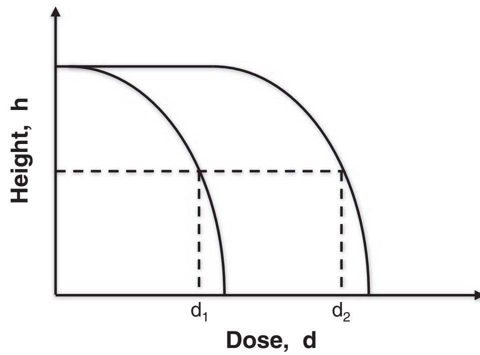

Fig. 2. The sketch illustrating application of eqs. (8) and (9) to extract the model parameters from experimental contrast curves. The doses are taken at the same height h. The height is related to dissolution depth z by $h = 1 - z/z_{\max}$.

$$\int_{z_1}^{z_2} f(z)\,dz = c\exp\left(-\frac{\Delta U}{kT_1}\right) d_1^{\alpha}\Delta t_1, \tag{6}$$

$$\int_{z_1}^{z_2} f(z)\,dz = c\exp\left(-\frac{\Delta U}{kT_2}\right) d_2^{\alpha}\Delta t_2, \tag{7}$$

for the first and second sample, respectively. Since the left-hand sides of eqs. (6) and (7) are identical, taking their ratio provides the following equation:

$$\Delta U = \frac{\alpha k T_1 T_2}{T_1 - T_2} \ln\left(\frac{d_2 \sqrt[\alpha]{\Delta t_2}}{d_1 \sqrt[\alpha]{\Delta t_1}}\right). \tag{8}$$

As can be seen, the depth dependence of the scission yield $p(z)$ is excluded from the equation. Similarly, for two samples exposed with different doses and developed up to the same depth with the same temperature $T_1 = T_2$, one obtains

$$\alpha = \frac{\ln(\Delta t_1/\Delta t_2)}{\ln(d_2/d_1)}. \tag{9}$$

In eqs. (8) and (9), Δt_1 and Δt_2 are development times for which the dissolution depths were measured, and d_1 and d_2 are the corresponding exposure doses. The equations allow estimation of the effective activation energy ΔU and the contrast parameter α from pairs of experimental contrast curves, taking the doses at the same height (which is equivalent to $z_{\max} - z$) as shown in Fig. 2. Equation (8) is applied to contrast curves obtained at different temperatures T_1 and T_2, whereas eq. (9) is applied to contrast curves obtained with the same temperature. Equation (8) can be employed for estimations of activation energy if α is known and eq. (9) provides an independent estimation of α. For a pair of contrast curves, eqs. (8) and (9) can be applied to a variety of heights, producing sets of multiple estimates for ΔU and α. Importantly, eqs. (8) and (9) do not depend on any details of the scission distribution within exposed resist, which makes them applicable to a broad variety of positive tone resists and developers, as well as scission and dissolution models.

In this work, we explore the outcomes of eq. (8) to get estimations of the effective activation energy with a number of assumed values of α from 2 to 10. For this purpose, we employ four experimental contrast curves for ZEP developed in MIBK : IPA 1 : 3, for two temperatures and two times of development as depicted at Fig. 1(b). These contrast curves are grouped in four pairs so that two curves in each pair correspond to different temperatures (see Table I, first row). Then, for each pair the estimations of activation energy are made at selected heights with fixed values of α as shown at Fig. 2. The idea is to find such values for activation energy and α (both supposed to be constant) to best fit all the experimental data. The results of fitting of the activation energy for two selected parameters α are presented in Table I. We also estimated α independently through eq. (9). Further discussion of these results is given in the next section.

Furthermore, we developed a detailed model to simulate contrast curves with accounting for both main chain scissioning by electron exposure and kinetic processes of development. Our model of exposure is a modification of the earlier approach,[15] which attributes main chain scissioning in ZEP to dissociative ionization occurring upon knocking out valence electrons involved in C–C binding in the main chain as well as in some of side groups. In distinction from the previous work,[15] which assumed the enhancement of the main-chain scission in ZEP by electron impact on both phenyl and chlorine groups, here we consider a milder scission enhancement upon electron impact only onto chlorine groups.[12,13] Other details of the exposure model are as described in ref. 15. Employing the resulting yields of the main-chain scissions, we compute the spatial distributions of fragments of various lengths in exposed resist as described in detail elsewhere.[30,31] The development process is represented by a sequence of discrete dissolution steps with time δt required to dissolve a resist layer of thickness δz at depth z determined by $\delta t = z\delta z/D(z)$ in accordance with eqs. (1) and (2). The simulation provides the location of the resist-developer interface as a function of development time for a given applied dose, given that parameters β_0, α and ΔU are known.

We parameterized the model, employing four experimental contrast curves for ZEP developed in MIBK : IPA 1 : 3 mixture [Fig. 1(b)]. First, for fixed temperatures and assumed values of α, we found best-fit values of $\beta = \beta_0 \exp(-\Delta U/kT)$ by minimizing the objective function for dissolution depth z,

$$F = \sum [z_{\text{computed}}(t,d) - z_{\text{experiment}}(t,d)]^2,$$

where the summation is performed over a representative set of experimental points from contrast curves. Then, by finding the best-fit ratios of β obtained at different temperatures of $T = -15$ and 22 °C, the activation energy ΔU was found. Table II lists the resulting ratios $\Delta U/\alpha$, and Figs. 3(a) and 3(b) present examples of the computed contrast curves for ZEP developed in MIBK : IPA 1 : 3.

4. Discussion

4.1 Contrast curve study

In this study, we obtain contrast curves for ZEP developed in ZED-N50, MIBK : IPA 1 : 3, and IPA : H_2O 7 : 3 at 22 and −15 °C for 5 and 20 s development times. Except for ZED-N50, which is the developer with the greatest affinity for ZEP amongst the current selection, the development times bear no effect on the contrast. For ZED-N50 developer at 22 °C, 5 s development time yields a higher contrast than 20 s at the cost of reduced sensitivity; however, we observe that cooling the developer down to −15 °C reduces the effect of varying development time as well.

 © 2012 The Japan Society of Applied Physics

Table I. The diffusion activation energies for ZEP developed in MIBK : IPA 1 : 3 mixture, obtained by fitting of eq. (8) to four pairs of contrast curves from Fig. 1(b) for two values of α.

Curves 5 s 22 °C/5 s −15 °C			Curves 5 s 22 °C/20 s −15 °C			Curves 20 s 22 °C/20 s −15 °C			Curves 20 s 22 °C/5 s −15 °C		
$h\%$	ΔU (eV)		$h\%$	ΔU (eV)		$h\%$	ΔU (eV)		$h\%$	ΔU (eV)	
	$\alpha = 2$	$\alpha = 10$		$\alpha = 2$	$\alpha = 10$		$\alpha = 2$	$\alpha = 10$		$\alpha = 2$	$\alpha = 10$
0.9724	0.22	1.12	0.9622	0.42	1.13	0.9622	0.18	0.91	0.9634	−0.057	0.70
0.9634	0.19	0.93	0.958	0.43	1.18	0.958	0.20	0.99	0.9606	−0.037	0.80
0.9606	0.20	1.01	0.9469	0.40	1.04	0.9469	0.21	1.03	0.9578	−0.016	0.90
0.9578	0.21	1.05	0.9392	0.42	1.12	0.9392	0.23	1.14	0.9461	−0.012	0.92
0.9461	0.19	0.93	0.8385	0.38	0.92	0.8385	0.22	1.08	0.9364	0.006	1.01
0.9364	0.20	0.99	0.4923	0.33	0.69	0.4923	0.12	0.58	0.8970	0.016	1.06
0.897	0.18	0.88	0.3189	0.34	0.70	0.3189	0.12	0.62	0.6821	−0.070	0.63
0.6821	0.14	0.70	0.2161	0.35	0.76	0.2161	0.14	0.69	0.4610	−0.085	0.56
0.461	0.13	0.65	0.1573	0.36	0.84	0.1573	0.16	0.78	0.3870	−0.069	0.64
0.387	0.14	0.70	0.1231	0.38	0.92	0.1231	0.17	0.87	0.3780	−0.050	0.73
0.378	0.16	0.80	0.1210	0.42	1.10	0.1210	0.21	1.05	0.2087	−0.049	0.73
0.2087	0.16	0.81	0.0825	0.43	1.17	0.0825	0.13	1.13	0.1811	−0.033	0.82
0.1811	0.18	0.88	0.0818	0.40	1.00	0.0818	0.19	0.95			
Average ΔU (eV)	0.18	0.88	Average ΔU (eV)	0.39	0.97	Average ΔU (eV)	0.18	0.91	Average ΔU (eV)	−0.04	0.79

Table II. Ratios $\Delta U/\alpha$ for different values of α obtained by fitting of the detailed resist dissolution model to experimental contrast curves for ZEP developed in MIBK : IPA 1 : 3 mixture.

α	$\Delta U/\alpha$ (eV)
2	0.06
6	0.08
8	0.08
10	0.08
12	0.08

Comparing the contrast curves for the aforementioned three developers and two developer temperatures in Fig. 1(a), we make a number of observations. For 22 °C development conditions, MIBK : IPA 1 : 3 yields the highest contrast; however, it yields nearly 4 times lower sensitivity compared to ZED-N50. IPA : H_2O 7 : 3 yields the lowest sensitivity (nearly 10 times lower than ZED-N50) and apparently does not yield pattern clearance as the contrast curve seems to exhibit a positive-to-negative tone transition at approximately 600 μC/cm^2. In addition, for MIBK : IPA 1 : 3 and IPA : H_2O 7 : 3 developers, we note that the contrast curve shoulder seems to exhibit a rapid dip and settling before resuming its normal behavior. Such a behavior has also been observed by Yang *et al.*[22] using IPA, which is a very weak developer for ZEP. This can be attributed to an uneven development where the scissioned polymer fragments are extracted from the dissolution front (interface) in aggregates in weak solvents. Figure 1(b) compares the room temperature (22 °C) and cold (−15 °C) development contrast curves using MIBK : IPA 1 : 3 developer at 5 and 20 s development times, respectively. The improvement of the contrast curve shoulder at −15 °C temperature demonstrates improvement in both 5 and 20 s development data sets.

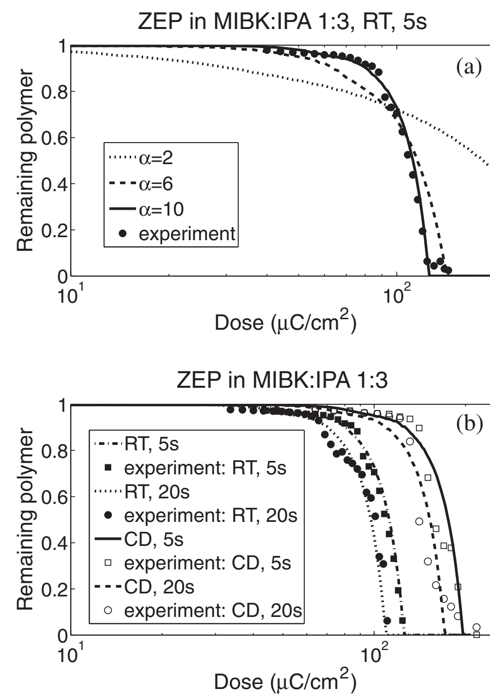

Fig. 3. Examples of computed contrast curves for ZEP developed in MIBK : IPA 1 : 3. (a) The best fit to experimental data for different values of parameter α, for room temperature development during 5 s. (b) Comparison of computed contrast curves for $\alpha = 10$ with experimental data obtained with 5 and 20 s durations and −15 and 22 °C temperatures of development.

Comparing the behavior of room temperature 22 °C development to cold −15 °C development, it is clear that the cold development improves the contrast for ZED-N50 and MIBK : IPA 1 : 3 developers at the expense of sensitivity. In the case of ZED-N50, the sensitivity penalty is nearly 3 times; however, in the case of MIBK : IPA 1 : 3, the difference is less than 2 times. In the case of MIBK : IPA 1 : 3 at −15 °C, we notice that the contrast

© 2012 The Japan Society of Applied Physics

curve tail is slightly raised. This behavior is contrary to expectation, and may point to a very early onset of competition between positive and negative tone behavior in ZEP. Observing the IPA : H_2O 7 : 3 contrast curve at $-15\,°C$, we notice a decrease in sensitivity and that only 40% clearance is achieved before tone-reversal takes place around $800\,\mu C/cm^2$. The contrast curve shoulders of both MIBK : IPA 1 : 3 and IPA : H_2O 7 : 3 developers are closer to the conventional expectation at cold $-15\,°C$ development temperature, signifying an improvement in contrast. In addition, we observe that the negative tone slope is nearly the same at equivalent doses regardless of developer temperature; however, for $-15\,°C$ development, the contrast curve negative tone behavior seems to saturate around $1100\,\mu C/cm^2$ showing that perhaps negative tone patterns are 20% shorter than positive tone patterns.

4.2 Modeling study

Theory in the present work aims to propose an efficient approach to predict the development process in electron beam lithography employing ZEP as a resist. For this purpose, a kinetic model of a diffusion-driven dissolution process is adopted as described in §3. Although by no means are our models limited to a particular resist-developer set, in this work we apply the models to development of ZEP in MIBK : IPA 1 : 3 mixture. As it follows from our experimental findings, the MIBK : IPA 1 : 3 mixture offers the advantage of improving both surface roughness and LER, as well as leads to successful clearance in a broad range of development temperatures. For these reasons, we consider development of ZEP in the MIBK : IPA mixture as an example.

Table I lists the effective activation energies ΔU obtained by fitting eq. (8) to four pairs of contrast curves for ZEP developed in MIBK : IPA 1 : 3 at two different temperatures and times of development [see Fig. 1(b)]. The results for two assumed values of $\alpha = 2$ and 10 are presented. Since the estimates obtained from different heights h produce somewhat different ΔU values, the average activation energies are also given for each pair of the curves. It can be seen that for $\alpha = 2$, the average ΔU values for different pairs of contrast curves vary from -0.04 to 0.39 eV, which is incompatible. More consistent estimates for activation energy are obtained when α increases. The best consistency for ZEP-520 developed with MIBK : IPA 1 : 3 was achieved with $\alpha = 10$ resulting in activation energy $\Delta U = 0.8\,eV$. In addition, we have also estimated α by applying eq. (9) to a pair of contrast curves obtained at ambient temperature. These estimates also predict large α values of about 10 or higher.

Independently, we have also performed the fitting of our detailed model of ZEP resist dissolution to experimental contrast curves from Fig. 1(b). Table II presents the best fit ratios $\Delta U/\alpha$ obtained with various α values. Interestingly, it turned out that the ratio $\Delta U/\alpha$ is insensitive to α, indicating that the activation energy depends on α almost linearly. In Fig. 3(a), the computed contrast curves obtained with various α are compared with experiment for the example of ZEP development in MIBK : IPA at room temperature for 5 s. Although the above ratio $\Delta U/\alpha$ is almost constant, the slope of computed contrast curves strongly depends on α, and the best compatibility is achieved for $\alpha = 10$. This corresponds to the activation energy $\Delta U = 0.8\,eV$, which is in good agreement with the complementary fitting for individual dissolution depths through eq. (8). As can be seen from Fig. 3(b), the computed contrast curves obtained with a single best-fit value of $\alpha = 10$ fit quite well to the entire set of experimental data obtained for ZEP development in MIBK : IPA 1 : 3 mixture. The slope of ZEP contrast curves appears to be largely independent on duration and temperature of development in this example.

These examples demonstrate that the rather complex process of ZEP resist dissolution can be described by a simple diffusion-driven model containing only three kinetic parameters. Both the suggested novel analytical approach and more detailed kinetic modeling of dissolution provide compatible results, indicating the effective activation energy of approximately 0.8 eV and the contrast parameter $\alpha \cong 10$. Such a large value of α is quite unexpected (see, for example, the discussion in ref. 28) and may indicate that the previously adopted[15,28] values of contrast parameter $\alpha \leq 2$ need to be revisited. Further research will allow elucidation of the underlying molecular mechanisms.

Table III. Surface roughness information for various developer and development conditions employed in this study for positive tone behavior (in nm).

Developer	Surface roughness	
	at 22 °C	at −15 °C
ZED-N50	8.1	12.7
MIBK : IPA 1 : 3	2.3	1.9
IPA : H_2O 7 : 3	3.1	2.6

4.3 Surface roughness study

In order to compare the various developers, we obtain high resolution (slow-scan) AFM micrographs of selected $1\,\mu m$ exposed squares used in the contrast curve study at similar trench depths. A $300 \times 300\,nm^2$ measurement box in the centre of the $1\,\mu m$ exposed square is used to calculate the RMS surface roughness tabulated in Table III. We observe that the surface roughness at room temperature conditions is highest for ZED-N50 at 8.1 nm and 2–3 times lower in MIBK : IPA 1 : 3 and IPA : H_2O 7 : 3 at 2.3 and 3.1 nm respectively. This result is intuitively expected as the strongest developer is also supposed to yield the largest surface roughness. Yamaguchi *et al.*[18] have demonstrated a correlation between surface roughness and van der Waals (vdW) volume of various alkyl-acetate developers of increasing molecular weight. They have hypothesized that a developer with a larger vdW volume yields a larger surface roughness. Whereas we also observe a similar correlation of surface roughness for our set of developers using the tables made available by Zhao *et al.*,[32] the interpretation based on vdW volumes alone may not be sufficient considering the tremendous complexity of the ZEP dissolution process.[12,15]

Comparing the cold $-15\,°C$ development and room $22\,°C$ temperature surface roughness behavior of all three developers, we observe that the surface roughness exhibits a small decrease except in the case of ZED-N50. The reduction in surface roughness with decreasing temperature for the weaker developers is expected and can be explained

© 2012 The Japan Society of Applied Physics

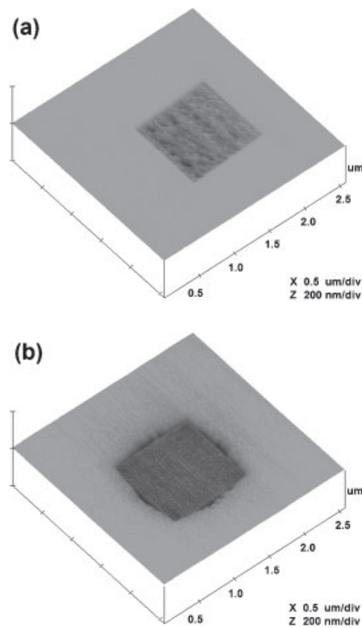

Fig. 4. Atomic force micrographs of 1 μm squares exposed at 10 keV and developed at −15 °C in IPA : H_2O 7 : 3 for 20 s. The measured surface roughness is (a) 2.6 nm, positive tone, and (b) 0.9 nm, negative tone. Both samples have a trench depth of 20–25 nm.

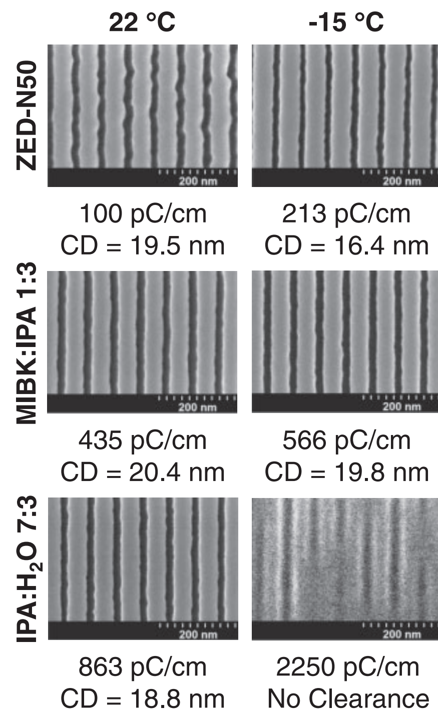

Fig. 5. Scanning electron micrographs of 70 nm pitch and 60 nm thick ZEP-520 gratings, exposed at 10 keV and developed for 5 s in ZED-N50, MIBK : IPA 1 : 3, and IPA : H_2O 7 : 3 developer at 22 and −15 °C development temperature. The applicable doses and CD for each combination are noted.

in terms of the dissolution kinetics; however, in the case of ZED-N50, this appears to be an anomaly. Since we are trying to measure the surface roughness at equivalent trench depths, perhaps the corresponding different exposure doses result in different dissolution dynamics. For example, the higher exposure dose might produce a higher percentage of voids in the scissioned resist.

In addition, we also compare the surface roughness of the positive tone versus negative tone behavior as shown in Fig. 4. For −15 °C development using the IPA : H_2O 7 : 3 developer at 20 s, we observe that the surface roughness of the scissioned resist (a: 2.6 nm) is nearly 3 times larger than the surface roughness of the cross-linked resist (b: 0.9 nm). Figure 4(b) is also interesting as the AFM micrograph clearly shows the square outline of the exposed and cross-linked area with rounded edges due to the proximity effect.

4.4 Dense gratings study

In order to evaluate the viability of the various developers in this study for patterning dense high resolution gratings, we conduct a number of experiments varying the pattern pitch, dose, development time and temperature. Figure 5 shows a representative set of 70 nm pitch gratings in 60 nm thick ZEP resist developed in ZED-N50, MIBK : IPA 1 : 3, and IPA : H_2O 7 : 3 developers at 22 and −15 °C developer temperatures for 5 s development time. Table IV lists the applicable doses for the above experimental conditions in both absolute and relative terms.

For 22 °C developer temperature, ZED-N50 is 4–8.5 times more sensitive compared to MIBK : IPA 1 : 3, and IPA : H_2O 7 : 3 developers. The critical dimension (CD) variation is less than 1.0 nm amongst these developers with IPA : H_2O 7 : 3 developer yielding the highest resolution of 18.8 nm. The line edge roughness (LER) for development in IPA : H_2O 7 : 3 and MIBK : IPA 1 : 3 is also visibly better

Table IV. Dose window information for various developer and development conditions employed in this study.

Developer	Dose window at 22 °C		Dose window at −15 °C	
	Values (pC/cm)	D_{max}/D_{min}	Values (pC/cm)	D_{max}/D_{min}
ZED-N50	100–205	2.05	213–525	2.46
MIBK : IPA 1 : 3	435–627	1.44	566–1212	2.14
IPA : H_2O 7 : 3	863–2356	2.73	No clearance	

compared to ZED-N50. The dose window for the latter (weaker) developers is also 8–15 times larger, showing greater process fidelity. Comparing −15 °C development to 22 °C development, we observe that ZED-N50 yields the greatest difference in CD of nearly 3 nm yielding 16.4 nm features at the cost of a twofold sensitivity decrease. Whereas, for MIBK : IPA 1 : 3, the CD improvement is less than 1 nm for a 1.3 times sensitivity decrease. The relative dose window increase with colder developer in both cases is 3–3.4 times, respectively. MIBK : IPA 1 : 3 developer provides successful clearance for a broad range of development temperatures along with the advantage of improved surface and line edge roughness.

In the case of IPA : H_2O 7 : 3 developer, no clearance was observed for the cold −15 °C development condition, which is expected in accordance with the contrast curve results in Fig. 1(a). For 22 °C development in IPA : H_2O 7 : 3 developer, the contrast curve also did not exhibit clearance (nearly 20% remaining), however, the gratings do exhibit clearance, which can be attributed to a number of factors such as different exposure step size (2 nm line step vs 20 nm area step), pattern geometry (dense exposure in one

© 2012 The Japan Society of Applied Physics

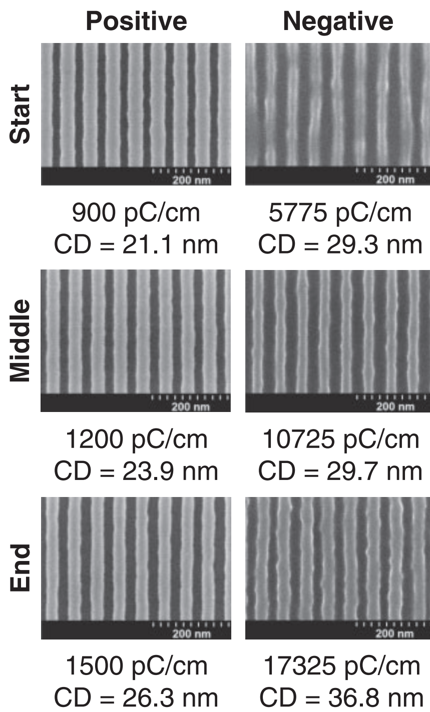

Fig. 6. Scanning electron micrographs of 60 nm pitch and 60 nm thick ZEP-520 gratings, exposed at 10 keV, and developed for 20 s in IPA : H_2O 7 : 3 developer at 22 °C. The micrographs are taken at the "start", "middle", and "end" of the dose window. The applicable doses and CD for each combination are noted.

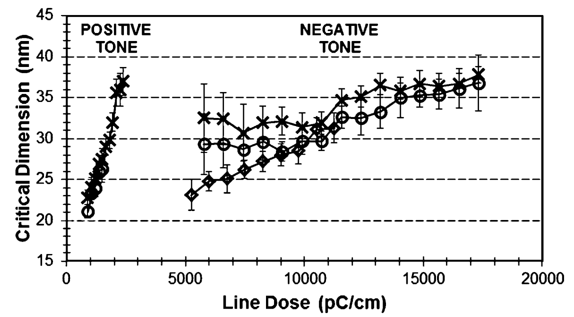

Fig. 7. Critical dimension versus line dose trend for 50 nm pitch (diamonds), 60 nm pitch (circles), and 70 nm pitch (crosses) gratings for both positive and negative tone behavior. The conditions used are 10 keV, 60 nm thick resist, 20 s IPA : H_2O 7 : 3 developer at 22 °C.

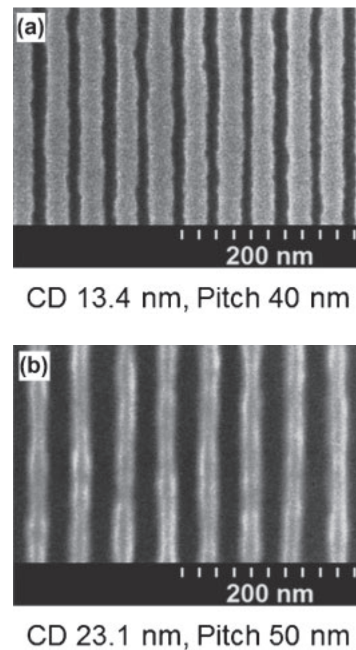

Fig. 8. Highest resolution/density patterns fabricated in this study using (a) 180 pC/cm, 5 s ZED-N50 at −15 °C and (b) 5250 pC/cm, 20 s IPA : H_2O 7 : 3 developer at 22 °C. The CD and pitch are noted.

line vs sparse area exposure), proximity threshold (greater charge accumulation removes scum), etc. In addition, for the 22 °C development in IPA : H_2O 7 : 3 developer, we also conducted successful lift-off experiments using 12 nm chromium metallization, to ensure complete clearance at the aforementioned process conditions.

4.5 Negative tone ZEP study

Recently, Oyama *et al.* have studied positive-to-negative tone inversion behavior of ZEP resist at high exposure doses using large area patterns and suggested mechanisms for this behavior.[33] In our present work, we studied the patterning of dense gratings using our alternative developer set. In Fig. 6, we show a representative set of 60 nm pitch positive and negative tone gratings in 60 nm thick resist developed in IPA : H_2O 7 : 3 for 20 s at 22 °C. The variation in CD is shown as we move from the start to the end of the applicable dose window. In the positive tone behavior, the CD increases from 21.1–26.3 nm in the dose window of 900–1500 pC/cm ($D_{max}/D_{min} \sim 1.67$); whereas in the negative tone behavior, the CD increases from 29.3–36.8 nm in the dose window of 5775–17325 pC/cm ($D_{max}/D_{min} \sim 3.0$). We also observe that various grating metrics such as line edge roughness (LER) and CD uniformity (CDU) visibly improve in the middle of the dose window regardless of tone.

A detailed CD versus line dose trend for 50, 60, and 70 nm pitch positive and negative tone gratings for 20 s IPA : H_2O development at 22 °C, is provided in Fig. 7, which yields some interesting observations. It can be seen that the CD is lower for denser gratings at the same exposure dose. Moreover this CD dependence on geometry (grating pitch) is stronger for negative tone patterns. The 60 nm pitch grating CD is, on average, 1 nm smaller for positive tone behavior and 2–3 nm smaller for negative tone behavior, as compared to 70 nm pitch gratings. Perhaps the larger accessible area in wider grating pitches allows for rapid diffusion, which may help explain the variation in CD. For the 50 nm pitch gratings, the positive tone trend is not available at all, whereas a detailed negative tone trend is available. As we noticed in the contrast curves, the negative tone gratings are expected to be 20% thinner, and hence with a less challenging aspect ratio (AR), the availability of dense 50 nm pitch gratings is explained at room temperature conditions.

Finally, Fig. 8 shows the highest resolution, densest features obtained in this study for both positive tone (a) and negative tone (b) behavior. The highest resolution positive tone features are 13 nm gaps in 40 nm pitch, yielding an aspect ratio of nearly 1 : 4.5 in 60 nm thick resist. This has been achieved using 5 s development in

© 2012 The Japan Society of Applied Physics

−15 °C ZED-N50. The highest resolution negative tone features are 23.1 nm lines in 50 nm pitch. This has been achieved using 20 s development in 22 °C IPA : H_2O 7 : 3. The smallest positive tone CD of 13 nm at 10 keV using ZEP/Silicon is state-of-the-art; it matches previously reported value of 13 nm outermost zone plate fabrication using ZEP 7000 on nitride membrane structure using 25 keV and −50 °C development (see ref. 24).

5. Summary

It is well known that the various performance metrics of an electron beam resist (e.g., sensitivity, contrast, resolution, etc.) depend strongly on the developer and development process. In this work, we compare the room (22 °C) and cold (−15 °C) development behavior of ZEP resist using ZED-N50, MIBK : IPA 1 : 3, and IPA : H_2O 7 : 3 developers through various experimental studies of contrast curves, dense gratings, and surface roughness measurements. In addition, we observe and characterize the negative tone behavior of ZEP in detail. The critical dimension and dose window for dense gratings is compared for both positive and negative tone behavior.

We also present an efficient approach to model the development process in electron beam lithography. For this purpose, a diffusion-driven kinetic model of development is adopted. For the case of uniform resist exposure, simple formulas are derived that allow parameterization of the development model from experimental contrast curves. The formulas do not depend on scission distribution within exposed resist, and as a consequence are applicable to a broad variety of process conditions. It is shown that the suggested modeling approach is effective enough so that a rather complex process of ZEP resist dissolution can be represented by a kinetic model containing only three microscopic parameters, which can be determined from experimental data. The dissolution model developed here can be applied to other resists and developers, as well as has the potential to be extended to negative tone resists. Our numerical analysis of the example of ZEP development in the MIBK : IPA 1 : 3 mixture indicates that the slope of ZEP contrast curves is largely independent on duration and temperature of development in this example.

Drawing specific conclusions from the entire set of experimental results obtained, we observe that at room temperature development, IPA : H_2O 7 : 3 provides the best resolution and LER followed by MIBK : IPA 1 : 3 and ZED-N50, at the expense of sensitivity. Cold (−15 °C) development improves the resolution and LER for ZED-N50 and MIBK : IPA 1 : 3 developers at near equivalent expense of sensitivity; however, it is not possible to achieve pattern clearance with IPA : H_2O 7 : 3 at −15 °C. Better surface roughness was achieved using MIBK : IPA 1 : 3 and IPA : H_2O 7 : 3 developers compared to ZED-N50 for both room temperature and cold development conditions. Finally, exposing ZEP by nearly an order higher magnitude of dose enables negative tone behaviour using IPA : H_2O 7 : 3 developer. For equivalent development conditions, negative tone ZEP gratings have a denser pitch, wider process window, and a lower surface roughness; however, the average critical dimension is greater than what can be achieved for positive tone ZEP gratings.

Acknowledgements

The authors would like to acknowledge Adegboyega Paul Adeyenuwo for his ImageJ script, the University of Alberta NanoFab, NINT Electron Microscopy group, and the support of NINT-NRC, NSERC, Alberta Innovates, iCORE, and NanoBridge.

1) J. G. Skinner, T. R. Groves, A. Novembre, H. Pfeiffer, and R. Singh: in *Handbook of Microlithography, Micromachining, and Microfabrication*, ed. P. Rai-Choudhury (SPIE, Bellingham, WA, 1997) Vol. 1, p. 425.
2) E. A. Dobisz, S. L. Brandow, R. Bass, and J. Mitterender: J. Vac. Sci. Technol. B **18** (2000) 107.
3) J. O. Choi, J. A. Moore, J. C. Corelli, J. P. Silverman, and H. Bakhru: J. Vac. Sci. Technol. B **6** (1988) 2286.
4) A. C. F. Hoole, M. E. Welland, and A. N. Broers: Semicond. Sci. Technol. **12** (1997) 1166.
5) S. Borini: J. Electrochem. Soc. **152** (2005) G482.
6) H. G. Duan, E. Q. Xie, and L. Han: J. Appl. Phys. **103** (2008) 046105.
7) S. Gautsch, M. Studer, and N. F. de Rooij: Microelectron. Eng. **87** (2010) 1139.
8) S. Gautsch and N. F. de Rooij: Microelectron. Eng. **88** (2011) 2533.
9) A. P. Adeyenuwo, M. Stepanova, and S. K. Dew: J. Vac. Sci. Technol. B **29** (2011) 06F312.
10) W. H. Teh and C. G. Smith: J. Vac. Sci. Technol. B **21** (2003) 3007.
11) H. Duan, J. Zhao, Y. Zhang, E. Xie, and L. Han: Nanotechnology **20** (2009) 135306.
12) T. Nishida, M. Notomi, R. Iga, and T. Tamamura: Jpn. J. Appl. Phys. **31** (1992) 4508.
13) H. Ikeura-Sekiguchi, T. Sekiguchi, and M. Koikea: J. Electron Spectrosc. Relat. Phenom. **144** (2005) 453.
14) T. Yamaguchi and H. Namatsu: J. Photopolym. Sci. Technol. **17** (2004) 557.
15) K. Koshelev, M. A. Mohammad, T. Fito, K. L. Westra, S. K. Dew, and M. Stepanova: J. Vac. Sci. Technol. B **29** (2011) 06F306.
16) ZEON Corporation Electronic Materials Division, ZEP520A Technical Report, ver. 2, Oct. 2010 [http://www.zeonchemicals.com/pdfs/ZEP520A.pdf] (last accessed 20 January 2012).
17) H. Namatsu, M. Nagase, K. Kurihara, K. Iwadate, and K. Murase: Microelectron. Eng. **27** (1995) 71.
18) T. Yamaguchi and H. Namatsu: J. Vac. Sci. Technol. B **22** (2004) 1037.
19) H. Wang, G. M. Laws, S. Milicic, P. Boland, A. Handugan, M. Pratt, T. Eschrich, S. Myhajlenko, J. A. Allgair, and B. Bunday: J. Vac. Sci. Technol. B **25** (2007) 102.
20) T. Okada, J. Fujimori, M. Aida, M. Fujimura, T. Yoshizawa, M. Katsumura, and T. Iida: J. Vac. Sci. Technol. B **29** (2011) 021604.
21) L. Ocola and A. Stein: J. Vac. Sci. Technol. B **24** (2006) 3061.
22) X. M. Yang, S. Xiao, W. Wu, Y. Xu, K. Mountfield, R. Rottmayer, K. Lee, D. Kuo, and D. Weller: J. Vac. Sci. Technol. B **25** (2007) 2202.
23) J. Reinspach, M. Lindblom, O. von Hofsten, M. Bertilson, H. M. Hertz, and A. Holmberg: J. Vac. Sci. Technol. B **27** (2009) 2593.
24) J. Reinspach, M. Lindblom, M. Bertilson, O. von Hofsten, H. M. Hertz, and A. Holmberg: J. Vac. Sci. Technol. B **29** (2011) 011012.
25) B. Cord, J. Lutkenhaus, and K. K. Berggren: J. Vac. Sci. Technol. B **25** (2007) 2013.
26) B. Cord: Ph. D. Thesis, Department of Electrical Engineering and Computer Science, Massachusetts Institute of Technology, Cambridge, MA, U.S.A (2009) [http://dspace.mit.edu/handle/1721.1/53267] (last accessed 20 January 2012).
27) ImageJ image analysis and processing software [http://rsbweb.nih.gov/ij/] (last accessed 20 January 2012).
28) M. A. Mohammad, T. Fito, J. Chen, M. Aktary, M. Stepanova, and S. K. Dew: J. Vac. Sci. Technol. B **28** (2010) L1.
29) M. A. Mohammad, T. Fito, J. Chen, S. Buswell, M. Aktary, M. Stepanova, and S. K. Dew: Microelectron. Eng. **87** (2010) 1104.
30) M. Stepanova, T. Fito, Zs. Szabo, K. Alti, A. P. Adeyenuwo, K. Koshelev, M. Aktary, and S. K. Dew: J. Vac. Sci. Technol. B **28** (2010) C6C48.
31) M. Aktary, M. Stepanova, and S. K. Dew: J. Vac. Sci. Technol. B **24** (2006) 768.
32) Y. H. Zhao, M. H. Abraham, and A. M. Zissimos: J. Org. Chem. **68** (2003) 7368.
33) T. G. Oyama, A. Oshima, H. Yamamoto, S. Tagawa, and M. Washio: Appl. Phys. Express **4** (2011) 076501.

© 2012 The Japan Society of Applied Physics